

# An improved RF cavity search for halo axions

S. J. Asztalos<sup>a</sup>, R. F. Bradley<sup>b</sup>, L. Duffy<sup>c</sup>, C. Hagmann<sup>a</sup>, D. Kinion<sup>a</sup>, D. M. Moltz<sup>d</sup>, L. J. Rosenberg<sup>a</sup>, P. Sikivie<sup>c</sup>, W. Stoeffl<sup>a</sup>, N. S. Sullivan<sup>c</sup>, D. B. Tanner<sup>c</sup>, K. van Bibber<sup>a</sup>, and D. B. Yu<sup>e</sup>

<sup>a</sup>Lawrence Livermore National Laboratory, Livermore, California 94550

<sup>b</sup>National Radio Astronomy Observatory, Charlottesville, Virginia 22903

<sup>c</sup>Department of Physics, University of Florida, Gainesville, Florida 32611

<sup>d</sup>Department of Chemistry, University of California, Berkeley, California 94720 and

<sup>e</sup>Department of Physics and Laboratory for Nuclear Science, Massachusetts Institute of Technology, Cambridge, Massachusetts 02139

(Dated: November 1, 2018)

The axion is a hypothetical elementary particle and cold dark matter candidate. In this RF cavity experiment, halo axions entering a resonant cavity immersed in a static magnetic field convert into microwave photons, with the resulting photons detected by a low-noise receiver. The ADMX Collaboration presents new limits on the axion-to-photon coupling and local axion dark matter halo mass density from a RF cavity axion search in the axion mass range 1.9–2.3  $\mu\text{eV}$ , broadening the search range to 1.9–3.3  $\mu\text{eV}$ . In addition, we report first results from an improved analysis technique.

PACS numbers: 14.80.Mz, 95.35.+d, 98.35.Gi

## I. INTRODUCTION

The axion is the pseudo-Goldstone boson [1, 2] implied by the Peccei-Quinn solution [3] to the “strong-CP” problem in QCD (for reviews, see, e.g., [4, 5]). The axion is also a good cold dark matter candidate [6, 7, 8], and could make a substantial contribution to the nearby galactic halo mass density, estimated to be approximately 0.45  $\text{GeV}/\text{cm}^3$  [9]. Axions are commonly thought to be thermalized, with energy virial width  $O(10^{-6})$  [10], and may be detected by the Sikivie RF cavity technique [11]. This paper describes new results from an ongoing RF cavity search by the ADMX (Axion Dark Matter eXperiment) Collaboration. We report limits based on predictions for the power  $P \sim g_{a\gamma\gamma}^2$  deposited in the cavity from two benchmark axion models, DFSZ [12, 13] and KSVZ [14, 15], where  $g_{a\gamma\gamma}$  is the effective coupling strength of axions to two photons [11].

## II. EXPERIMENT

The experimental apparatus has been described elsewhere [16]. Briefly, halo axions couple to the electric field in a tunable resonant cavity plus a DC magnetic field provided by a superconducting solenoid surrounding the cavity volume. The signal is excess power in the cavity when the frequency of the  $\text{TM}_{010}$  mode is close to the energy of the halo axions. The electric field in the cavity is coupled by an antenna probe to an ultra-low-noise cryogenic preamplifier, followed by further amplification, mixing, and digitization [17, 18]. Figure 1 shows a sketch of the detector and Figure 2 a schematic diagram of the receiver chain.

The magnet is a superconducting solenoid of 7.9 T central field. The RF cavity is a circular cylinder (50 cm diameter, 100 cm long) constructed of stainless steel plated with copper and subsequently annealed. The un-

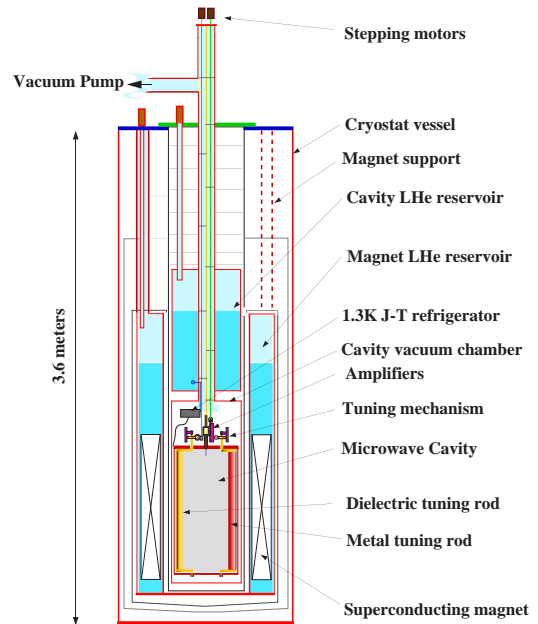


FIG. 1: Sketch of the RF cavity axion detector.

loaded cavity quality factor  $Q$  is approximately 200,000 at a resonant frequency of 500 MHz. In recent running, the temperature of the cavity was 1.6 K. The frequency of the cavity mode is tuned with a pair of axial tuning rods (metal or dielectric) that can be translated from near the cavity center to the wall.

For our most recent run, we used one metal tuning rod ( $d \sim 7.5$  cm) and one ceramic dielectric tuning rod ( $d \sim 5.0$  cm), with the ceramic rod fixed near the cavity center. With this tuning rod configuration, we were able to tune from 461–550 MHz, corresponding to axion masses 1.9–2.3  $\mu\text{eV}$ .

The cryogenic gain of the receiver comes from balanced GaAs HFET preamplifiers built by the National

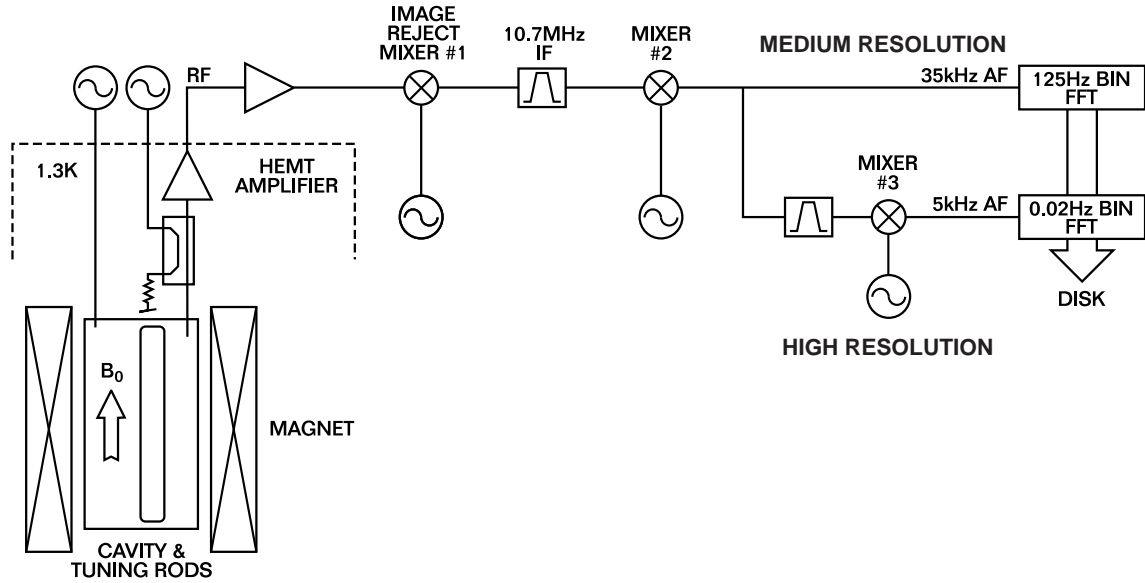


FIG. 2: Schematic diagram of the receiver chain.

Radio Astronomy Observatory [19]. At the operating temperature of 1.6 K, they have a noise temperature of approximately 1.9 K and power gain of 17 dB. The amplifier noise temperature was deduced by employing the warmed, critically coupled cavity as a Nyquist source. Due to their improved noise performance compared to earlier preamplifiers, the system noise temperature (sum of cavity physical temperature and electronic noise temperature) is significantly improved, producing a factor of 2 increase in the search rate relative to earlier operation [17, 18].

Data were collected from 08 July 2002 through 27 May 2003 in the form of “medium resolution” single-sided power spectra. Each spectrum consists of 10000 averaged, 400-bin, 125 Hz/bin subspectra, with each spectrum having 80 seconds of exposure. After each 80-second spectrum, the cavity frequency was tuned downwards by approximately 1 kHz. There is also a dedicated hardware channel optimized for detecting very narrow axion lines; results from this channel are not reported here.

Each frequency bin appears in 15 to 25 power spectra, corresponding to an averaging time of about 25 minutes. The receiver is stable over a much longer time, as demonstrated in figure 3. This figure shows the single-bin rms power divided by the average power versus the number of averages (lower abscissa) and the averaging time in days (upper abscissa). The log-log slope is approximately  $-1/2$  until  $10^{8.5}$  averages, corresponding to 30 days of continuous averaging; this establishes the ultimate single-bin sensitivity of the receiver, corresponding to  $\sim 10^{-26}$  Watts, or approximately 1 RF photon per minute at the signal frequency.

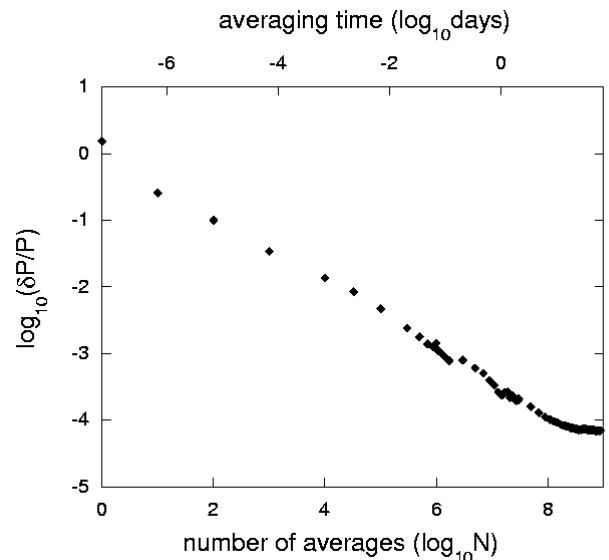


FIG. 3: Receiver power sensitivity ( $\log_{10} \delta P/P$ ) versus number of averages ( $\log_{10} N$ ) [lower abscissa] or averaging time ( $\log_{10}$  days) [upper abscissa].

### III. DATA ANALYSIS AND RESULTS

The receiver transfer function was calibrated by recording spectra with a precision noise source at the receiver input. Each cavity spectrum was corrected with this receiver calibration. The center 175 bins of each spectrum were then corrected with a 5-parameter equivalent-circuit model characterizing the cavity, transmission line, and amplifier interaction. Subsequently, spectra were linearly combined with a bin-by-bin weight-

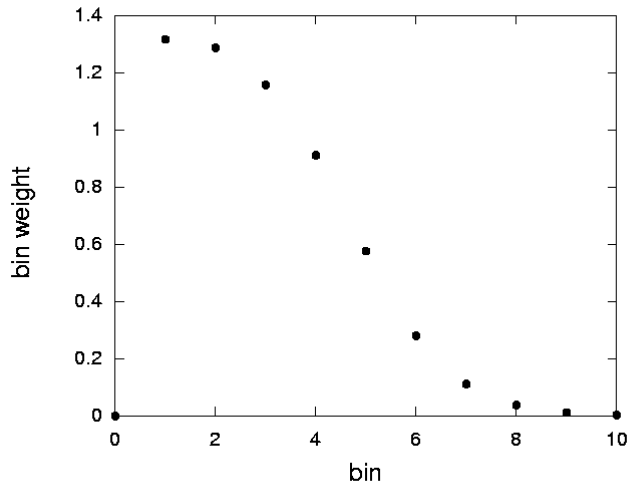


FIG. 4: Wiener filter weighting for axion mass corresponding to 500 MHz. The normalization is discussed in the text.

ing that accounts for that bin’s contribution to a thermalized axion signal. More details can be found in [16, 17].

This resulting medium resolution combined power spectrum was used in two parallel analyses. The first analysis created a power spectrum that was the sum of every 6 adjacent bins of the combined power spectrum, as was done previously [16, 17]. The second analysis, first suggested in [20], is newly reported here, and applied a Wiener filter (WF) [21] derived from the thermalized near-Maxwellian axion signal lineshape [10], whose output formed another power spectrum.

The output of the WF is a bin-by-bin sum with weighting

$$W(\nu) = \frac{S^2(\nu)}{S^2(\nu) + N^2(\nu)} \quad (1)$$

where  $S(\nu)$  and  $N(\nu)$  are the expected signal and noise powers in each frequency bin of the combined power spectrum (by contrast, the first analysis weights 6 adjacent bins with unity and others zero). The WF was normalized so as to nearly match the number of candidates from the 6-bin search at the same candidate threshold.

Figure 4 shows a WF weighting for an axion mass corresponding to 500 MHz. The abscissa represents the 125 Hz frequency bin offset from 500 MHz and the ordinate the WF weight.

We compared the WF and 6-bin sensitivity by simulating three different signal lineshapes on Gaussian noise: the thermalized near-Maxwellian lineshape, a narrow single-bin lineshape (developing power in one bin), and a 10-bin wide lineshape (developing power uniformly in 10 adjacent bins). For the narrow lineshape, the WF is more sensitive than the 6-bin filter; this is expected because the WF is narrower. For the wide lineshape, the

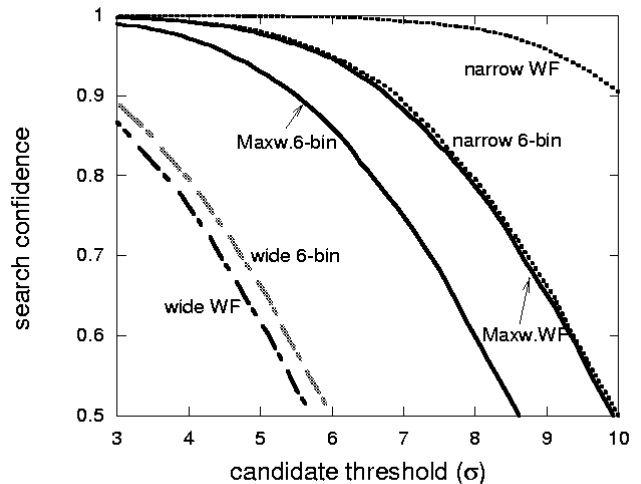


FIG. 5: Search confidence for finding thermalized axions (solid), narrow 1-bin wide axions (dotted), and wide 10-bin wide axions (dashed), from WF and 6-bin searches.

WF is slightly less sensitive. This is demonstrated in figure 5, which shows search confidence versus candidate threshold in units of single-bin rms power (as in [16, 17]). Sensitivity to narrow lineshapes is important, as narrow structures are predicted to accompany galaxy formation [22].

Candidates were selected separately from both analyses. The 6-bin threshold was chosen so as to have the analysis sensitive to thermalized KSVZ axions at 94% confidence, established via Monte Carlo technique. The WF threshold was selected to yield the same or slightly fewer number of candidates than the 6-bin search at the same confidence. There were 3159 6-bin candidates and 2974 WF candidates (1473 appeared in common), consistent with the expectation from system noise.

More data were taken at just these candidate frequencies so as to nearly double the effective integration time. Of these candidates, 176 6-bin candidates and 187 WF candidates (76 candidates in common) passed a second candidate threshold (chosen to maintain greater than 93% search confidence for thermalized KSVZ axions). Yet more data were taken at these surviving candidate frequencies, and candidates again were selected. Of these candidates, 12 6-bin candidates and 13 WF candidates (10 candidates in common) persisted. The number of candidates from these successive stages were approximately consistent with expectations from system noise.

At very high search confidence, ten of the 15 persistent candidates did not reappear after integrating for over 2 hours at each candidate frequency. These candidates are therefore highly unlikely to be axions. The remaining five candidates (common to both filters) reappeared after this long integration. These five candidate frequen-

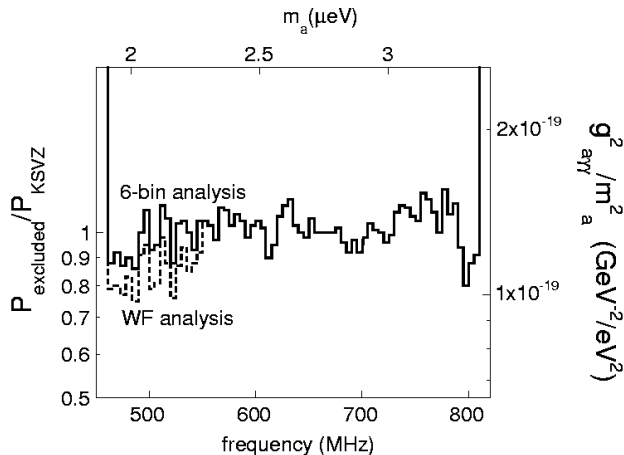


FIG. 6: Upper limit on axion-to-photon conversion power and coupling  $g_{a\gamma\gamma}$ , excluded at greater than 90% confidence.

cies were reexamined after removing a 20 dB attenuator at a calibration port. The power at each candidate frequency increased by roughly 100-fold, consistent with the removal of the attenuator and the hypothesis that these candidates are due to environmental RF contamination. In a further study, the cavity was replaced by a stub antenna connected to the input of the receiver. These same five candidates were also seen in these background power spectra. The attenuation and stub antenna studies suggest these remaining candidates are interfering external signals and are therefore rejected as axions.

Figure 6 shows axion-to-photon couplings excluded at greater than 90% confidence across our search range. The upper and lower abscissas represent axion mass and corresponding microwave photon frequency; the left and right ordinates represent power sensitivity in units of expected thermalized KSVZ axion power, and the axion-to-photon coupling  $g_{a\gamma\gamma}$  divided by axion mass  $m_a$ . The solid line is the 6-bin analysis upper limit, and the dotted line is the WF analysis upper limit. The WF analysis was not applied to frequencies greater than 550 MHz.

These results also constrain the local axion dark matter halo mass density [23]. Figure 7 shows the axion halo mass density excluded at greater than 90% confidence for thermalized KSVZ and DFSZ axions. The upper and lower abscissas represent axion mass and corresponding microwave photon frequency; the ordinate represents local axion dark matter mass density. The lower pair of

lines are upper limits for KSVZ axions; the upper pair of lines are upper limits for the weaker-coupled DFSZ axions. Solid lines are upper limits obtained from the 6-bin analysis; dotted lines are the upper limits obtained from the more sensitive WF analysis.

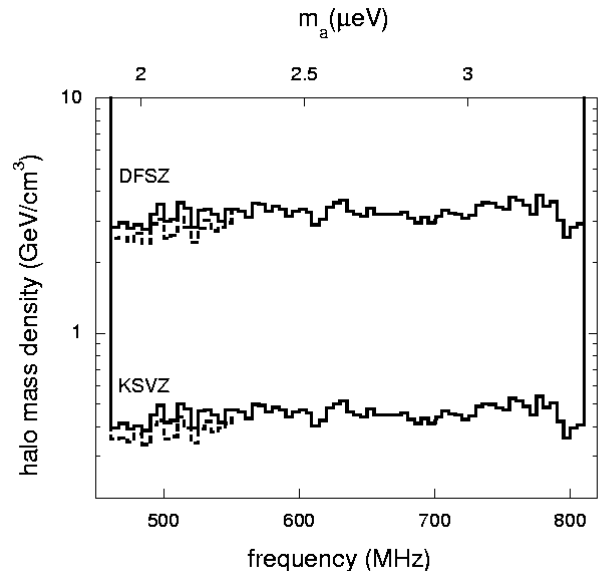


FIG. 7: Upper limits on galactic axion dark matter halo mass density excluded at greater than 90% confidence for KSVZ and DFSZ axions using the two analyses described in the text.

#### IV. CONCLUSION

In conclusion, we now exclude at greater than 90% confidence a KSVZ halo axion of mass 1.9–3.3  $\mu\text{eV}$ , assuming axions saturate the local dark matter halo. We also exclude at greater than 90% confidence a local axion dark matter halo mass density of greater than 0.45  $\text{GeV}/\text{cm}^3$  ( $\sim 3 \text{ GeV}/\text{cm}^3$ ) for KSVZ (DFSZ) axions. Improvements to this experiment come from lower noise preamplifiers; scanning is faster by a factor of 2. The analysis is also improved; the resulting power sensitivity gain from the WF is approximately 13%, representing an increased effective integration time of about 25%.

This work was performed under the auspices of the U.S. Department of Energy by the University of California, Lawrence Livermore National Laboratory under Contract W-7405-ENG-48, and the University of Florida under grant DE-FG02-97ER41209.

- [1] S. Weinberg, Phys. Rev. Lett. **40**, 223 (1978).
- [2] F. Wilczek, Phys. Rev. Lett. **40**, 279 (1978).
- [3] R. D. Peccei and H. R. Quinn, Phys. Rev. Lett. **38**, 1440 (1977).
- [4] J. Kim, Phys. Rep. **150**, 1 (1997).
- [5] H.-Y. Cheng, Phys. Rep. **158**, 1 (1998).

- [6] J. Preskill, M. Wise, and F. Wilczek, Phys. Lett. B **120**, 127 (1983).
- [7] L. Abbott and P. Sikivie, Phys. Lett. B **130**, 133 (1983).
- [8] M. Dine and W. Fischler, Phys. Lett. **B120**, 137 (1983).
- [9] E. I. Gates, G. Gyuk, and M. S. Turner, Astrophys. J. **449**, 123 (1995).

- [10] M. Turner, Phys. Rev. D **42**, 3572 (1990).
- [11] P. Sikivie, Phys. Rev. Lett. **51**, 1415 (1983).
- [12] M. Dine, W. Fischler, and M. Srednicki, Phys. Lett. **104B**, 199 (1981).
- [13] A. P. Zhitnitskii, Sov. J. Nucl. Phys. **31**, 260 (1980).
- [14] J. Kim, Phys. Rev. Lett. **43**, 103 (1979).
- [15] M. A. Shifman, A. I. Vainshtein, and V. I. Zakharov, Nucl. Phys. **B166**, 493 (1980).
- [16] H. Peng et al., Nucl. Instrum. Methods Phys. Res. A **444**, 569 (2000).
- [17] S. Asztalos et al., Phys. Rev. D **64**, 092003 (2001).
- [18] C. Hagmann et al., Phys. Rev. Lett. **80**, 2043 (1998).
- [19] E. Daw and R. F. Bradley, J. Appl. Phys. **82**, 1925 (1997).
- [20] L. Krauss, J. Moody, F. Wilczek, and D. E. Morris, Phys. Rev. Lett. **55**, 1797 (1985).
- [21] W. H. Press et al., *Numerical Recipes in C* (Cambridge University Press, 1992), 2nd ed.
- [22] P. Sikivie, I. I. Tkachev, and Y. Wang, Phys. Rev. Lett. **75**, 2911 (1995).
- [23] S. J. Asztalos et al., Astrophys. J. **571**, L27 (2002).